IEEE Access
Multidisciplinary | Rapid Review | Open Access Journal

Received July 10, 2020, accepted July 15, 2020, date of publication July 20, 2020, date of current version July 31, 2020.

*Digital Object Identifier 10.1109/ACCESS.2020.3010648*

# A Novel Sequential Sampling Algorithm for Reliability Assessment of Microgrids

**XIAOTONG SONG[1], YI SUN[1], FEI WANG[2], AND WENYUE XU[1]**
[1]School of Electrical and Control Engineering, North China University of Technology, Beijing 100144, China
[2]State Grid Shandong Electric Power Company, Jinan 250001, China

Corresponding author: Xiaotong Song (songxt@ncut.edu.cn)

**ABSTRACT** Due to the polymorphic uncertainties in microgrids (MGs), prohibitive computational burden is produced in reliability assessment. In this work, a novel sequential sampling algorithm (NSSA) compatible with sequential Monte Carlo (SMC) simulation is developed to overcome the computational burden. First, optimal probability density functions (PDFs) of random variables are worked out based on variation method. Then, optimal PDFs are employed to chronologically simulate the random states of microturbine (MT), photovoltaics (PV) and time varying load with improved computational efficiency. Therefore, the convergence of reliability assessment is accelerated accordingly. A series of case studies have been conducted, and the computational results show that NSSA provides a favorable sampling efficiency and adaptability to system conditions in reliability assessment of MGs. At last, based on optimal PDFs produced by NSSA, dominant joint PDF (DJ-PDF) is defined and employed to quantify the contributions of different scenarios to the reliability indices. Case studies have confirmed that DJ-PDF can provide detailed information for scenario-based reliability analysis.

**INDEX TERMS** Microgrid, sequential sampling, reliability assessment, computational efficiency, coefficient of variation.

## NOMENCLATURE

### *RANDOM VARIABLES*

| | |
|---|---|
| $u$ | random variable sampled for random operation hours |
| $v$ | random variable sampled for random repairing hours |
| $q$ | random variable defined to model time varying load |
| $p$ | random variable defined to model intermittency of PV |

### *INDICES AND SETS*

| | |
|---|---|
| $w_u$, $W_u$ | index and number of subintervals of [0, 1] on $u$-axis |
| $w_v$, $W_v$ | index and number of subintervals of [0, 1] on $v$-axis |
| $w_q$, $W_q$ | index and number of subintervals of [0, 1] on $q$-axis |
| $w_p$, $W_p$ | index and number of subintervals of [0, 1] on $p$-axis |

### *FUNCTIONS AND FUNCTIONAL*

| | |
|---|---|
| $f_u(u)$ | probability density function (PDF) of u |
| $f_v(v)$ | PDF of $v$ |
| $f_q(q)$ | PDF of $q$ |
| $f_p(p)$ | PDF of $p$ |
| $f_u^*(u)$ | optimal PDF of $u$ |
| $f_v^*(v)$ | optimal PDF of $v$ |
| $f_q^*(q)$ | optimal PDF of $q$ |
| $f_p^*(p)$ | optimal PDF of $p$ |
| $\tilde{f}_u^*(u^{(w_u)})$ | estimate of $f_u^*(u)$ on the $w_u$-th subinterval of [0, 1] |
| $\tilde{f}_v^*(v^{(w_v)})$ | estimate of $f_v^*(v)$ on the $w_v$-th subinterval of [0, 1] |
| $\tilde{f}_q^*(q^{(w_q)})$ | estimate of $f_q^*(q)$ on the $w_q$-th subinterval of [0, 1] |
| $\tilde{f}_p^*(p^{(w_p)})$ | estimate of $f_p^*(p)$ on the $w_p$-th subinterval of [0, 1] |
| $F_R(\cdot)$ | reliability test function in terms of $u$, $v$, $q$ and $p$ with uniform PDFs |
| $F'_R(\cdot)$ | reliability test function in terms of $u$, $v$, $q$ and $p$ with varying PDFs |

The associate editor coordinating the review of this manuscript and approving it for publication was Zhiyi Li.

$G_R(\cdot)$ reliability test function in terms of the hourly states of MT, PV and load
$F_L[\cdot]$ Functional in terms of $f_u(u)$, $f_v(v)$, $f_q(q)$ and $f_p(p)$

## I. INTRODUCTION

Reliability assessment of microgrids (MGs) has attracted more and more interests, since a growing number of customers are powered by MGs in a more flexible and environment-friendly way [1]–[3]. However, the ubiquitous issues with polymorphic uncertainties, such as stochastic operation cycles of MG components, intermittent output of distributed generators (DGs) and time varying load, etc., impose heavy computational burden on the reliability assessment of MGs [4].

Analytical method and Monte Carlo (MC) simulation, including the non-sequential Monte Carlo (NSMC) simulation and sequential Monte Carlo (SMC) simulation, are the basic methodologies in the reliability assessment of power system [5]. Although analytical method is favored for its efficiency in study on small systems, but is strongly limited or even forbidden for its rapidly growing computational cost when large scale systems with numerous random issues are concerned. Moreover, accuracy of analytical method is reduced since all high order contingencies are usually ignored. At last, its incompatibility with chronological issues also strictly limits the applications [6]. Compared with analytical method, MC simulation provides a more straightforward approach to model the components with uncertainties [7], and is preferred for its convergence performance which is independent on the system scale.

When NSMC simulation is employed, only the non-chronological random states of MG rather than the chronological ones can be obtained. As a result, it is difficult to consider the chronological issues in the reliability assessment. On the contrary, SMC simulation is preferred for its capability to accurately deal with chronological issues of MGs, such as operation cycles of components, intermittent output of DGs, time varying load, charge and discharge sequences of energy storage system (ESS), etc. Motivated by the aforementioned advantages of SMC simulation over the other available methods, considerable literatures adopted SMC method to conduct the reliability assessment of MGs [8]–[12].

It is well known that computational cost of MC simulation will increase rapidly when the requirement of simulation accuracy gets higher. Coefficient of variation (CV) is taken as a criteria to quantitatively measure the accuracy of MC simulation [13]. Due to the correlation between CV and variance of test function, CV can be effectively decreased by reducing the variance of test function without increasing computational cost [14]. In the field of main grids, a series of improved algorithms aiming at variance reduction in NSMC-based reliability assessment has been developed [15]. Importance sampling technique, for example, is proposed to reduce the variance by tracking the sampling volume with largest magnitude of test function [16]–[18]. By subdividing the sampling volume into smaller sub-volumes and changing their sizes, stratified sampling technique can supply a minimized variance when the contributions to the variance from each sub-volume are identical [19]. The limitations of importance sampling and stratified sampling are the requirement of detailed knowledge of the reliability function over different random variables, which is usually unavailable. Reference [20] proposes an optimal sampling algorithm, in which the probability density functions (PDFs) of random variables are optimized in the preliminary sampling process, and then optimal PDFs are utilized in the following reliability assessment process with accelerated convergence. The improved algorithms mentioned above are developed for NSMC simulation in reliability assessment of main grids. When it comes to SMC simulation in reliability assessment of MGs, however, these improved algorithms cannot be used directly, since the sampling mechanisms of SMC and NSMC are absolutely different. On the other hand, efficient sampling techniques are required more urgently when SMC simulation is applied, since the 'crude' SMC converges more slowly than NSMC [21].

To fill these gaps, within the context of standalone MG, an novel sequential sampling algorithm (NSSA) with high computational efficiency and compatibility with chronological issues has been developed. The contributions of the paper are as follows:

(a) Stochastic operation cycles of MG components, time varying load and intermittent photovoltaics (PV), *et al.*, are uniformly modeled by the functions of continuous random variables. Then multidimensional integration model of MG reliability assessment based on SMC simulation is proposed.

(b) The variance-reducing mechanisms are thoroughly analyzed, followed with analytical solutions of optimal PDFs. NSSA is thereafter developed to deal with the prohibitive computational burden produced by the polymorphic uncertainties of MGs.

(c) A series of case studies on test system is implemented and the convergence performances of NSSA are studied. The computational efficiency and adaptability of NSSA are confirmed by the results of case studies.

(d) A novel index, i.e., dominant joint PDF (DJ-PDF) is defined based on optimal PDFs. DJ-PDF is then proposed to quantify the contributions of different scenarios to the reliability indices and discriminate the critical scenarios with higher risk of load interruptions.

The remainder of the paper is organized as follows. Section II formulates the multidimensional integration model of MG reliability assessment. In section III, optimal PDFs of random variables are analytically worked out, and NSSA is developed. Computational efficiency and adaptability of NSSA are investigated based on intensive case studies in section IV, followed by conclusions of the paper in section V.

## II. MULTIDIMENSIONAL INTEGRATION MODEL OF MG RELIABILITY ASSESSMENT

### A. COMPONENTS' STOCHASTIC AND CHRONOLOGICAL OPERATION CYCLES

Stochastic and chronological operation cycles of MG components are composed of a series of operational periods and repairing periods. Take MT for example. Stochastic and chronological operation cycles are produced by (1) [7].

$$\begin{cases} TTF(u_i) = -\left(\dfrac{1}{\lambda}\right)\ln u_i \\ TTR(v_i) = -\left(\dfrac{1}{\mu}\right)\ln v_i \end{cases} \tag{1}$$

where, $TTF(u_i)$ and $TTR(v_i)$ are operational period and repairing period of the *i-th* operation cycle, $\lambda$ and $\mu$ are failure rate and repair rate of MT, $u_i$ and $v_i$ are the *i-th* sampling values of random variable $u$ and $v$. The operation cycles of MT are determined by PDFs of $u$ and $v$, which are denoted as $f_{\mathrm{u}}(u)$ and $f_{\mathrm{v}}(v)$. In traditional SMC simulation, continuous uniform PDFs are employed. In this work, $f_{\mathrm{u}}(u)$ and $f_{\mathrm{v}}(v)$ will be optimized to improve the simulation efficiency.

### B. QUARTERLY VARYING LOAD

With different time varying natures, hourly varying model, monthly varying model, quarterly varying model or annual peak load model, *et al.*, can be employed in the reliability assessment [14], [22], [23]. A load model with smaller time scale will result in more precise results but higher computational cost. In this paper, quarterly varying load $P_{\mathrm{LOAD}}(h)$ is employed and defined in (2).

$$P_{\mathrm{LOAD}}(h) = \begin{cases} P_{\mathrm{peak}} \times P_{\mathrm{cq}}^{(1)} h \in (0, h_{\mathrm{q}}^{(1)}) \\ P_{\mathrm{peak}} \times P_{\mathrm{cq}}^{(2)} h \in (h_{\mathrm{q}}^{(1)}, h_{\mathrm{q}}^{(1)} + h_{\mathrm{q}}^{(2)}) \\ P_{\mathrm{peak}} \times P_{\mathrm{cq}}^{(3)} h \in (h_{\mathrm{q}}^{(1)} + h_{\mathrm{q}}^{(2)}, h_{\mathrm{q}}^{(1)} + h_{\mathrm{q}}^{(2)} + h_{\mathrm{q}}^{(3)}) \\ P_{\mathrm{peak}} \times P_{\mathrm{cq}}^{(4)} h \in (h_{\mathrm{q}}^{(1)} + h_{\mathrm{q}}^{(2)} + h_{\mathrm{q}}^{(3)}, 8760) \end{cases} \tag{2}$$

where, $h$ is the number of simulation hours, $P_{\mathrm{cq}}^{(1)}$, $P_{\mathrm{cq}}^{(2)}$, $P_{\mathrm{cq}}^{(3)}$ and $P_{\mathrm{cq}}^{(4)}$ are the percentages of quarterly load in terms of the annual peak load $P_{\mathrm{peak}}$, $h_{\mathrm{q}}^{(1)}$, $h_{\mathrm{q}}^{(2)}$ and $h_{\mathrm{q}}^{(3)}$ are duration hours of quarter-1, quarter-2 and quarter-3, respectively. Let's define a random variable $q$ with PDF $f_{\mathrm{q}}(q)$ which is defined as follows:

$$f_{\mathrm{q}}(q) = \begin{cases} \eta_1 & q \in [0, 0.25) \\ \eta_2 & q \in [0.25, 0.5) \\ \eta_3 & q \in [0.5, 0.75) \\ \eta_4 & q \in [0.75, 1] \\ 0 & \text{otherwise} \end{cases} \tag{3}$$

Then, $h_{\mathrm{q}}^{(1)}$, $h_{\mathrm{q}}^{(2)}$ and $h_{\mathrm{q}}^{(3)}$ are worked out by multiplying 8760 hours by the probabilities that $q$ will be chosen from the first, second and third subintervals, respectively [24]:

$$h_{\mathrm{q}}^{(w_{\mathrm{q}})} = \mathrm{round}(\eta_{w_{\mathrm{q}}} \times 0.25 \times 8760), (w_{\mathrm{q}} = 1, 2, 3) \tag{4}$$

From (2), (3) and (4), we can see that the load has been modeled as a function of $q$. When $\eta_1$, $\eta_2$, $\eta_3$ and $\eta_4$ are equal to 1, duration hours of all the quarters will be identical. In this work, $\eta_{w_{\mathrm{q}}}$ will be elaborately optimized to improve the computational efficiency and as a result, duration hours of all the quarters will be changed accordingly.

### C. INTERMITTENT AND STOCHASTIC NATURES OF PV

PV power is characterized by its intermittent and stochastic natures and denoted as $P_{\mathrm{PV}}(h)$, which is specified as below,

$$P_{\mathrm{PV}}(h) = \begin{cases} 0 & c(h) \in [0, C_{\mathrm{PV}}^{(\mathrm{r})}) \\ P_{\mathrm{PV}}^{\mathrm{available}} & c(h) \in [C_{\mathrm{PV}}^{(\mathrm{r})}, C_{\mathrm{PV}}^{(\mathrm{s})}) \\ 0 & c(h) \in [C_{\mathrm{PV}}^{(\mathrm{s})}, 24] \end{cases} \tag{5}$$

where, $c(h)$ is the function that transforms the *h-th* simulation hour into a 24-hour clock, $P_{\mathrm{PV}}^{\mathrm{available}}$ is the PV power between sunrise time denoted as $C_{\mathrm{PV}}^{(\mathrm{r})}$ and sunset time denoted as $C_{\mathrm{PV}}^{(\mathrm{s})}$. It can be seen from (5) that the intermittent nature of PV is determined by $C_{\mathrm{PV}}^{(\mathrm{r})}$ and $C_{\mathrm{PV}}^{(\mathrm{s})}$, and the stochastic nature of PV is determined by the PDF of $P_{\mathrm{PV}}^{\mathrm{available}}$, which can be specified by Beta function [25], for example.

The computational efficiency can be improved by elaborately changing $C_{\mathrm{PV}}^{(\mathrm{r})}$ and $C_{\mathrm{PV}}^{(\mathrm{s})}$, since the intermittent nature of PV contributes to the variances of reliability indices. Let's divide 24 hours of one day into, for example, 8 time segments. Duration hours of the $w_{\mathrm{p}}$-*th* ($w_{\mathrm{p}}$ =1, 2,..., 8) time segment is denoted as $h_{\mathrm{p}}^{(w_{\mathrm{p}})}$. Then, $C_{\mathrm{PV}}^{(\mathrm{r})}$ and $C_{\mathrm{PV}}^{(\mathrm{s})}$ can be assumed as

$$\begin{cases} C_{\mathrm{PV}}^{(\mathrm{r})} = h_{\mathrm{p}}^{(1)} + h_{\mathrm{p}}^{(2)} \\ C_{\mathrm{PV}}^{(\mathrm{s})} = 24\text{-}(h_{\mathrm{p}}^{(7)} + h_{\mathrm{p}}^{(8)}) \end{cases} \tag{6}$$

A random variable $p$ is defined to represent the intermittency of PV [24], and PDF of $p$ denoted as $f_{\mathrm{p}}(p)$ is specified as

$$f_{\mathrm{p}}(p) = \begin{cases} \xi_1 & p \in [0, 0.125) \\ \xi_2 & p \in [0.125, 0.25) \\ \cdots & \cdots \\ \xi_{w_{\mathrm{p}}} & p \in [(w_{\mathrm{p}} - 1) \times 0.125, w_{\mathrm{p}} \times 0.125) \\ \cdots & \cdots \\ \xi_8 & p \in [0.875, 1] \\ 0 & \text{otherwise} \end{cases} \tag{7}$$

where $\xi_{w_{\mathrm{p}}}$ is value of $f_{\mathrm{p}}(p)$ in the $w_{\mathrm{p}}$-*th* subinterval. It can be seen from (7) that $f_{\mathrm{p}}(p)$ is defined as a piecewise function and specified on 8 subintervals according to the number of time segments. Furthermore, $h_{\mathrm{p}}^{(w_{\mathrm{p}})}$ will be worked out by multiplying 24 hours by the probabilities that $p$ is chosen from the $w_{\mathrm{p}}$-*th* subinterval:

$$h_{\mathrm{p}}^{(w_{\mathrm{p}})} = \mathrm{round}(\xi_{w_{\mathrm{p}}} \times 0.125 \times 24) \tag{8}$$

$C_{\mathrm{PV}}^{(\mathrm{r})}$ and $C_{\mathrm{PV}}^{(\mathrm{s})}$ are determined by $f_{\mathrm{p}}(p)$ according to (6), (7) and (8). If $\xi_{w_{\mathrm{p}}}$ is equal to 1, for example, then $C_{\mathrm{PV}}^{(\mathrm{r})}$ and $C_{\mathrm{PV}}^{(\mathrm{s})}$ are set to 6:00 and 18:00 accordingly. In other words, the intermittency of PV will be depicted by the single random variable $p$ with proper PDF.

### D. INDEPENDENCE OF RANDOM VARIABLES

The independence of aforementioned random variables, such as $u$, $v$, $q$ and $p$, should be considered, since the stochastic performance of MGs are determined by the joint PDFs of random variables. Firstly, $u$ and $v$ are both independent of other random variables due to the assumption that the component outages are independent random events [26]. Secondly, the correlation between $q$ and $p$ is determined by the time scales of PV and load. As shown in (5), the cycle of PV intermittency is 24 hours. On the other hand, the cycle of load fluctuation shown in (2) is 8760 hours, which is much larger than the cycle of PV intermittency. Cycles of PV intermittency are limited within 24 hours and contained in the cycles of quarterly load. As a result, the changes of quarterly load profile will have little influence on the profile of PV, and vice versa. Therefore, it can be concluded that the correlation of $q$ and $p$ is weak and marginal when quarterly varying load is employed. When it comes to the monthly varying load or even the weekly varying load model, similar conclusions can be drawn. When the time scale of load model is less than 24 hours and comparable to the time scale of PV, however, correlation of $q$ and $p$ will be strong due to the time dependence and cannot be ignored anymore. In this situation, the correlation of PV and load can still be properly dealt with by defining one random variable to simultaneously model the PV and load over time segments. In this way, the algorithm developed in this paper will not be prohibited by the correlation of random variables.

### E. MULTIDIMENSIONAL INTEGRATION MODEL OF MG RELIABILITY

As stated in Subsection A, B and C, the polymorphic uncertainties of MT, load and PV are modeled by random variables $u$, $v$, $q$ and $p$ with uniform PDFs on the interval of [0, 1]. In other words, PDFs of $u$, $v$, $q$ and $p$ are equal to 1 on the interval of [0, 1] and equal to 0 otherwise. Reliability index $R$ can be thereafter expressed as the expectation value of its test function,

$$R = \int_{\Omega} F_{\mathrm{R}}\left(u, v, q, p\right) du \cdot dv \cdot dq \cdot dp \tag{9}$$

where $F_{\mathrm{R}}(\cdot)$ is the test function in terms of $u$, $v$, $q$ and $p$, and integration volume $\Omega$ is a hypercube with unit side length. $R$ cannot be worked out analytically due to the absence of analytical expression of $F_{\mathrm{R}}(\cdot)$, but can be estimated based on MC integration methodology instead [27]. When changed PDFs of $u$, $v$, $q$ and $p$, i.e., $f_{\mathrm{u}}(u)$, $f_{\mathrm{v}}(v)$, $f_{\mathrm{q}}(q)$ and $f_{\mathrm{p}}(p)$ rather than uniform PDFs are employed in the sampling process, test function will be revised accordingly.

$$F'_{\mathrm{R}}(u, v, q, p) = \frac{F_{\mathrm{R}}(u, v, q, p)}{f_{\mathrm{u}}(u) f_{\mathrm{v}}(v) f_{\mathrm{q}}(q) f_{\mathrm{p}}(p)} \tag{10}$$

where, $F'_{\mathrm{R}}(\cdot)$ is the revised test function corresponding to $f_{\mathrm{u}}(u)$, $f_{\mathrm{v}}(v)$, $f_{\mathrm{q}}(q)$ and $f_{\mathrm{p}}(p)$. Then, reliability index $R$ will be worked out as follows.

$$R = \int_{\Omega} F'_{\mathrm{R}}\left(u, v, q, p\right) f_{\mathrm{u}}(u) f_{\mathrm{v}}(v) f_{\mathrm{q}}(q) f_{\mathrm{p}}(p) du \cdot dv \cdot dq \cdot dp \tag{11}$$

It can be seen from (9), (10) and (11) that unbiased value of $R$ can be obtained even from $f_{\mathrm{u}}(u)$, $f_{\mathrm{v}}(v)$, $f_{\mathrm{q}}(q)$ and $f_{\mathrm{p}}(p)$ instead of uniform PDFs, provided that test function is revised according to (10). However, variance will be produced differently by MC integration when different $f_{\mathrm{u}}(u)$, $f_{\mathrm{v}}(v)$, $f_{\mathrm{q}}(q)$ and $f_{\mathrm{p}}(p)$ are employed.

$$\begin{cases} V_{\mathrm{R}} = V'_{\mathrm{R}} - R^2 \\ V'_{\mathrm{R}} = \displaystyle\int_{\Omega} \frac{F^2_{\mathrm{R}}\left(u, v, q, p\right)}{f_{\mathrm{u}}(u) f_{\mathrm{v}}(v) f_{\mathrm{q}}(q) f_{\mathrm{p}}(p)} du \cdot dv \cdot dq \cdot dp \end{cases} \tag{12}$$

where, $V_{\mathrm{R}}$ is the variance produced by MC integration according to (11). As specified in (12), $V_{\mathrm{R}}$ is composed of 2 parts, i.e., $V_{\mathrm{R}}$' and $R^2$. Since CV is taken as a criteria of the computational efficiency and reduced along with $V_{\mathrm{R}}$, the variance reduction technique is then studied in the following section.

## III. NSSA DEVELOPED FOR MG RELIABILITY ASSESSMENT

### A. ANALYTICAL SOLUTIONS OF OPTIMAL PDFS

In (12), $R$ is a constant, and therefore $V_{\mathrm{R}}$ and $V_{\mathrm{R}}$' will get the minimum values simultaneously by optimizing $f_{\mathrm{u}}(u)$, $f_{\mathrm{v}}(v)$, $f_{\mathrm{q}}(q)$ and $f_{\mathrm{p}}(p)$. Variation method is used to work out the analytical solutions of optimal PDFs. Note that $V_{\mathrm{R}}$' is a functional of $f_{\mathrm{u}}(u)$, $f_{\mathrm{v}}(v)$, $f_{\mathrm{q}}(q)$ and $f_{\mathrm{p}}(p)$. With the objective of minimization of $V_{\mathrm{R}}$' and equality constrains of $f_{\mathrm{u}}(u)$, $f_{\mathrm{v}}(v)$, $f_{\mathrm{q}}(q)$ and $f_{\mathrm{p}}(p)$, the computation of optimal PDFs can be formulated as follows.

$$\begin{aligned} &\text{obj. } \min\left\{V'_R\right\} \\ &\text{s.t.} \begin{cases} \displaystyle\int_0^1 f_{\mathrm{u}}(u) du = 1 \\ \displaystyle\int_0^1 f_{\mathrm{v}}(v) dv = 1 \\ \displaystyle\int_0^1 f_{\mathrm{q}}(q) dq = 1 \\ \displaystyle\int_0^1 f_{\mathrm{p}}(p) dp = 1 \end{cases} \end{aligned} \tag{13}$$

The functional problem in terms of extreme value mentioned above is solved by variation method. Firstly, a new functional denoted as $F_{\mathrm{L}}[\cdot]$ is constructed based on $V_{\mathrm{R}}$' and Lagrange multipliers.

$$\begin{aligned} &F_{\mathrm{L}}\left[f_{\mathrm{u}}(u), f_{\mathrm{v}}(v), f_{\mathrm{q}}(q), f_{\mathrm{p}}(p)\right] \\ &\quad = V'_R + \Lambda_{\mathrm{u}} \int_0^1 f_{\mathrm{u}}(u) du \\ &\qquad + \Lambda_{\mathrm{v}} \int_0^1 f_{\mathrm{v}}(v) dv + \Lambda_{\mathrm{q}} \int_0^1 f_{\mathrm{q}}(q) dq + \Lambda_{\mathrm{p}} \int_0^1 f_{\mathrm{p}}(p) dp \end{aligned} \tag{14}$$

where, $\Lambda_{\mathrm{u}}$, $\Lambda_{\mathrm{v}}$, $\Lambda_{\mathrm{q}}$ and $\Lambda_{\mathrm{p}}$ are Lagrange multipliers. Then the optimal solutions of PDFs denoted as $f^*_{\mathrm{u}}(u)$, $f^*_{\mathrm{v}}(v)$, $f^*_{\mathrm{q}}(q)$

and $f_{\mathrm{p}}^{*}(p)$ are worked out by solving Euler equation [24]. The analytical solutions of $f_{\mathrm{u}}^{*}(u), f_{\mathrm{v}}^{*}(v), f_{\mathrm{q}}^{*}(q)$ and $f_{\mathrm{p}}^{*}(p)$ are specified in (15).

$$\begin{cases} f_{\mathrm{u}}^{*}(u) = \dfrac{\sqrt{I_{\mathrm{u}}(u)}}{\int_0^1 \sqrt{I_{\mathrm{u}}(u)}du} \\ f_{\mathrm{v}}^{*}(v) = \dfrac{\sqrt{I_{\mathrm{v}}(v)}}{\int_0^1 \sqrt{I_{\mathrm{v}}(v)}dv} \\ f_{\mathrm{q}}^{*}(q) = \dfrac{\sqrt{I_{\mathrm{q}}(q)}}{\int_0^1 \sqrt{I_{\mathrm{q}}(q)}dq} \\ f_{\mathrm{p}}^{*}(p) = \dfrac{\sqrt{I_{\mathrm{p}}(p)}}{\int_0^1 \sqrt{I_{\mathrm{p}}(p)}dp} \end{cases} \tag{15}$$

where,

$$\begin{cases} I_{\mathrm{u}}(u) = \iiint_{\Omega_{\mathrm{u}}} \dfrac{F_{\mathrm{R}}^{2}(u,v,q,p)}{f_{\mathrm{v}}(v)f_{\mathrm{q}}(q)f_{\mathrm{p}}(p)}dv \cdot dq \cdot dp \\ I_{\mathrm{v}}(v) = \iiint_{\Omega_{\mathrm{v}}} \dfrac{F_{\mathrm{R}}^{2}(u,v,q,p)}{f_{\mathrm{u}}(u)f_{\mathrm{q}}(q)f_{\mathrm{p}}(p)}du \cdot dq \cdot dp \\ I_{\mathrm{q}}(q) = \iiint_{\Omega_{\mathrm{q}}} \dfrac{F_{\mathrm{R}}^{2}(u,v,q,p)}{f_{\mathrm{u}}(u)f_{\mathrm{v}}(v)f_{\mathrm{p}}(p)}du \cdot dv \cdot dp \\ I_{\mathrm{p}}(p) = \iiint_{\Omega_{\mathrm{p}}} \dfrac{F_{\mathrm{R}}^{2}(u,v,q,p)}{f_{\mathrm{u}}(u)f_{\mathrm{v}}(v)f_{\mathrm{q}}(q)}du \cdot dv \cdot dq \end{cases} \tag{16}$$

where, $\Omega_{\mathrm{u}}$, $\Omega_{\mathrm{v}}$, $\Omega_{\mathrm{q}}$ and $\Omega_{\mathrm{p}}$, are unit cubes in coordinate systems of *v-p-q*, *u-p-q*, *u-v-p* and *u-v-q*, respectively [20].

### B. ESTIMATION OF OPTIMAL PDFs OF U AND V

Stochastic and chronological operation cycles of MT, are determined by random variables $u$, $v$ and their PDFs. The contribution of MT to the variance will be minimized by sampling from optimal PDFs of $u$ and $v$. However, the absence of analytical expression of $F_{\mathrm{R}}(\cdot)$ prohibits us from using $f_{\mathrm{u}}^{*}(u)$ and $f_{\mathrm{v}}^{*}(v)$ directly. Then, piecewise functions are defined as follows to estimate $f_{\mathrm{u}}^{*}(u)$ and $f_{\mathrm{v}}^{*}(v)$.

$$\begin{cases} \tilde{f}_{\mathrm{u}}^{*}\left(u^{(w_{\mathrm{u}})}\right) = \dfrac{\sqrt{\tilde{I}_{\mathrm{u}}(u^{(w_{\mathrm{u}})})}}{\frac{1}{W_{\mathrm{u}}}\sum_{t=1}^{W_{\mathrm{u}}}\sqrt{\tilde{I}_{\mathrm{u}}(u^{(t)})}}, \quad (w_{\mathrm{u}} = 1,\ 2,\ \ldots,\ W_{\mathrm{u}}) \\ \tilde{f}_{\mathrm{v}}^{*}\left(v^{(w_{\mathrm{v}})}\right) = \dfrac{\sqrt{\tilde{I}_{\mathrm{v}}(v^{(w_{\mathrm{v}})})}}{\frac{1}{W_{\mathrm{v}}}\sum_{t=1}^{W_{\mathrm{v}}}\sqrt{\tilde{I}_{\mathrm{v}}(u^{(t)})}}, \quad (w_{v} = 1,\ 2,\ \ldots,\ W_{\mathrm{v}}) \end{cases} \tag{17}$$

where, intervals of [0, 1] on $u$-axis and $v$-axis are uniformly divided into $W_{\mathrm{u}}$ and $W_{\mathrm{v}}$ subintervals, and $W_{\mathrm{u}}$ and $W_{\mathrm{v}}$ are identically set to 5 in the following case studies. $\tilde{f}_{\mathrm{u}}^{*}(u^{(w_{\mathrm{u}})})$ and $\tilde{I}_{\mathrm{u}}(u^{(w_{\mathrm{u}})})$ are the estimates of $f_{\mathrm{u}}^{*}(u)$ and $I_{\mathrm{u}}(u)$ on the $w_{\mathrm{u}}$-*th* subinterval of [0, 1] on $u$-axis, and $\tilde{f}_{\mathrm{v}}^{*}(v^{(w_{\mathrm{v}})})$ and $\tilde{I}_{\mathrm{v}}(v^{(w_{\mathrm{v}})})$ are the estimates of $f_{\mathrm{v}}^{*}(v)$ and $I_{\mathrm{v}}(v)$ on the $w_{\mathrm{v}}$-*th* subinterval of [0, 1] on $v$-axis. $\tilde{I}_{\mathrm{u}}(u^{(w_{\mathrm{u}})})$ and $\tilde{I}_{\mathrm{v}}(v^{(w_{\mathrm{v}})})$ can be worked out by sequential samplings in similar ways. Hence, only the computation of $\tilde{I}_{\mathrm{u}}(u^{(w_{\mathrm{u}})})$ is stated in this work. Firstly, $\tilde{I}_{\mathrm{u}}(u^{(w_{\mathrm{u}})})$ is expressed as follows according to (16) and MC integration methodology [27]:

$$\tilde{I}_{\mathrm{u}}(u^{(w_{\mathrm{u}})}) = \frac{1}{N_{\mathrm{v}}N_{\mathrm{u}}^{(w_{\mathrm{u}})}}\sum_{i=1}^{N_{\mathrm{u}}^{(w_{\mathrm{u}})}}\sum_{j=1}^{N_{\mathrm{v}}}\frac{F_{\mathrm{R}}^{2}(u_i, v_j, q, p)}{f_{\mathrm{v}}(v)f_{\mathrm{q}}(q)f_{\mathrm{p}}(p)}, \quad u_i \in \left(\frac{w_{\mathrm{u}}-1}{W_{\mathrm{u}}}, \frac{w_{\mathrm{u}}}{W_{\mathrm{u}}}\right) \tag{18}$$

where, $N_{\mathrm{v}}$ is the sample number of $v$ on [0, 1], and $N_{\mathrm{u}}^{(w_{\mathrm{u}})}$ is the sample number of $u$ produced on the $w_{\mathrm{u}}$-*th* subinterval of [0, 1]. Secondly, as shown in (19), $F_{\mathrm{R}}(u_i, v_j, q, p)$ is estimated by another test function $G_{\mathrm{R}}(\cdot)$ in terms of the hourly random states of MT, PV and load, given that analytical solution of $F_{\mathrm{R}}(\cdot)$ is unavailable.

$$\begin{aligned} &F_{\mathrm{R}}\left(u_i, v_j, q, p\right) \\ &= [\sum_{k=1}^{TTF(u_i)} G_{\mathrm{R}}(P_{\mathrm{mt}}, P_{\mathrm{LOAD}}(TTF(u_i)_k), P_{\mathrm{PV}}(TTF(u_i)_k)) \\ &\quad \times \left|_{P_{\mathrm{mt}}=P_{\mathrm{MT}}} + \sum_{k=1}^{TTR(v_j)} G_{\mathrm{R}}(P_{\mathrm{mt}}, P_{\mathrm{LOAD}}(TTR(v_j)_k),\right. \\ &\quad \left. P_{\mathrm{PV}}(TTR(v_j)_k)\right|_{P_{\mathrm{mt}}=0}]/[TTF(u_i) + TTR(v_j)] \end{aligned} \tag{19}$$

where, $P_{\mathrm{mt}}$ and $P_{\mathrm{MT}}$ are the available power and rated capacity of MT, respectively. During the hours of $TTF(u_i)$, MT is in normal states with $P_{\mathrm{mt}}$ which is equal to $P_{\mathrm{MT}}$. During the hours of $TTR(v_j)$, MT is in fault states with $P_{\mathrm{mt}}$ which is equal to 0. $TTF(u_i)_k$ and $TTR(v_j)_k$ are the hourly sequence numbers of the $k$-*th* hours in $TTF(u_i)$ and $TTR(v_j)$, respectively. The stochastic and chronological operation cycles of MT are graphically shown in Fig. 1.

Finally, $G_{\mathrm{R}}(\cdot)$ can be solved by states analysis of MG system. Take, for example, the reliability index of loss of load probability (LOLP) [28]. $G_{\mathrm{R}}(\cdot)$ is worked out as follows:

$$G_{\mathrm{R}}(P_{\mathrm{mt}}, P_{\mathrm{LOAD}}, P_{\mathrm{PV}}) = \begin{cases} 1 & \text{if } P_{\mathrm{mt}} + P_{\mathrm{PV}} + P_{\mathrm{ESS}} < P_{\mathrm{LOAD}} \\ 0 & \text{otherwise} \end{cases} \tag{20}$$

where, $P_{\mathrm{ESS}}$ is the power capacity of ESS. As shown in (20), $G_{\mathrm{R}}(\cdot)$ is computed by assessing the ability of MT, PV and ESS (if available) etc. to power the load. According to (17)-(20), $f_{\mathrm{u}}^{*}(u)$ will be estimated by SMC simulation, and $f_{\mathrm{v}}^{*}(v)$ can also be estimated in a similar way.

### C. ESTIMATION OF OPTIMAL PDF OF Q

Random variable $q$ and its PDF determine the profile of quarterly varying load. The optimal PDF of $q$ can be estimated by piecewise function as follows:

$$\tilde{f}_{\mathrm{q}}^{*}\left(q^{(w_{\mathrm{q}})}\right) = \frac{\sqrt{\tilde{I}_{\mathrm{q}}(q^{(w_{\mathrm{q}})})}}{\frac{1}{W_{\mathrm{q}}}\sum_{t=1}^{W_{\mathrm{q}}}\sqrt{\tilde{I}_{\mathrm{q}}(q^{(t)})}}, (w_{\mathrm{q}} = 1,\ 2,\ \ldots,\ W_{\mathrm{q}}) \tag{21}$$

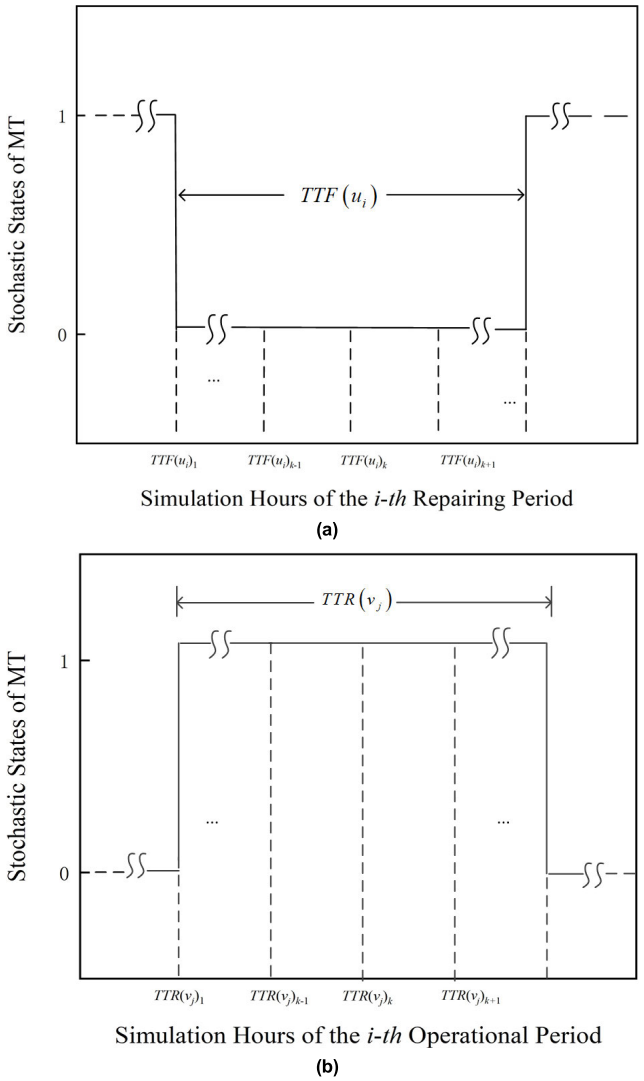


**FIGURE 1.** Stochastic and chronological operation cycles of MT. (a) During TTF($u_i$), MT is in the normal states represented by 0, and (b) During of TTR($v_j$), MT is in the fault states represented by 1.

where, interval of [0, 1] on $q$-axis is uniformly divided into $W_q$ subintervals, and $W_q$ is set to 4 since quarterly load is considered. $\tilde{f}_q^*(q^{(w_q)})$ and $\tilde{I}_q(q^{(w_q)})$ are the estimates of $f_q^*(q)$ and $I_q(q)$ on the $w_q$-*th* subinterval of [0, 1] on $q$-axis. $\tilde{I}_q(q^{(w_q)})$ is worked out as follows:

$$\tilde{I}_q(q^{(w_q)}) = \frac{1}{N_q^{(w_q)}} \sum_{i=1}^{N_q^{(w_q)}} \frac{F_R^2(u, v, q_i, p)}{f_u(u) f_v(v) f_p(p)}, \quad q_i \in \left(\frac{w_q - 1}{W_q}, \frac{w_q}{W_q}\right) \tag{22}$$

where, $N_q^{(w_q)}$ is the sample number of $q$ on the $w_q$-*th* subinterval of [0, 1], and is identical to the number of quarter-$w_q$ contained in the simulation. Here, $F_R(u, v, q_i, p)$ is estimated by $G_R(\cdot)$ as follows:

$$\begin{aligned} &F_R(u, v, q_i, p) \\ &= \frac{1}{h_q^{(w_q)}} \sum_{k=1}^{h_q^{(w_q)}} G_R(P_{mt}(C_q(i, w_q, k)), P_{peak} \\ &\quad \times P_{cq}^{(w_q)}, P_{PV}(C_q(i, w_q, k))) \end{aligned} \tag{23}$$

where, $P_{peak} \times P_{cq}^{(w_q)}$ is the load during $h_q^{(w_q)}$, and $C_q(i, w_q, k)$ is the hourly sequence number of the $k$-*th* hour in quarter-$w_q$ of the $i$-*th* simulation year. The profile of quarterly varying load as well as the aforementioned variables are graphically shown in Fig. 2.

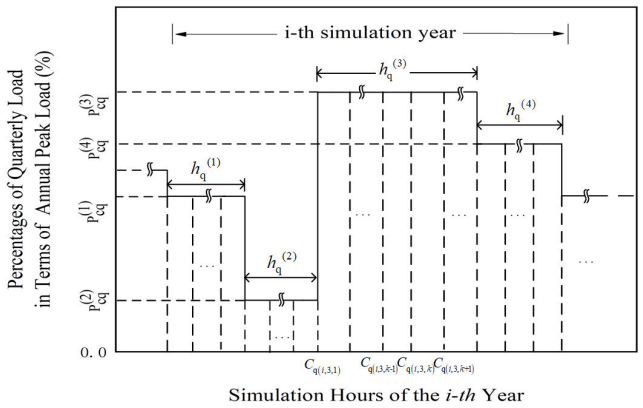


**FIGURE 2.** Hourly profile of quarterly varying load. Duration hours of quarters are determined and changed when necessary by PDF of $q$.

According to (21)-(23), estimate of $f_q^*(q)$ will be worked out by SMC simulation. With decision of optimal PDF of $q$, the load profile reshaped for an improved computational efficiency is also determined accordingly. It should be noted that, although quarterly varying load model is applied in this paper, the algorithm can be extended to monthly or even hourly varying models straightforwardly.

### D. ESTIMATION OF OPTIMAL PDF OF P

Random variable $p$ and its PDF will determine the intermittent performance of PV, which are characterized by $C_{PV}^{(r)}$ and $C_{PV}^{(s)}$. The optimal PDF of $p$, i.e., $f_p^*(p)$ can be estimated by piecewise function as follows:

$$\tilde{f}_p^*\left(p^{(w_p)}\right) = \frac{\sqrt{\tilde{I}_p(p^{(w_p)})}}{\frac{1}{W_p}\sum_{t=1}^{W_p}\sqrt{\tilde{I}_p(p^{(t)})}}, \quad (w_p = 1, 2, \ldots, W_p) \tag{24}$$

where, interval of [0, 1] on $p$-axis is uniformly divided into $W_p$ subintervals, and $W_p$ is set to 8 in this paper. $\tilde{f}_p^*(p^{(w_p)})$ and $\tilde{I}_p(p^{(w_p)})$ are the estimates of $f_p^*(p)$ and $I_p(p)$ on the $w_p$-*th* subinterval of [0, 1], respectively. $\tilde{I}_p(p^{(w_p)})$ can be worked out

by MC integration methodology as follows:

$$\tilde{I}_{\mathrm{p}}(p^{(w_{\mathrm{p}})}) = \frac{1}{N_{\mathrm{p}}^{(w_{\mathrm{p}})}} \sum_{i=1}^{N_{\mathrm{p}}^{(w_{\mathrm{p}})}} \frac{F_{\mathrm{R}}^2(u, v, q, p_i)}{f_{\mathrm{u}}(u) f_{\mathrm{v}}(v) f_{\mathrm{q}}(q)}, \quad p_i \in \left(\frac{w_{\mathrm{p}}-1}{W_{\mathrm{p}}}, \frac{w_{\mathrm{p}}}{W_{\mathrm{p}}}\right) \tag{25}$$

where, $N_{\mathrm{p}}^{(w_{\mathrm{p}})}$ is the sample number of $p$ on the $w_{\mathrm{p}}$-*th* subinterval of [0, 1], and is also identical to the number of $w_{\mathrm{p}}$-*th* time segments contained in the SMC simulation. Here, $F_{\mathrm{R}}(u, v, q, p_i)$ is estimated by $G_{\mathrm{R}}(\cdot)$ as follows:

$$\begin{aligned} F_{\mathrm{R}}(u, v, q, p_i) &= \frac{1}{h_{\mathrm{p}}^{(w_{\mathrm{p}})}} \\ &\times \sum_{k=1}^{h_{\mathrm{p}}^{(w_{\mathrm{p}})}} G_{\mathrm{R}}(P_{\mathrm{mt}}(C_{\mathrm{p}}(i, w_{\mathrm{p}}, k)), \\ &P_{\mathrm{LOAD}}(C_{\mathrm{p}}(i, w_{\mathrm{p}}, k)), P_{\mathrm{PV}}(C_{\mathrm{p}}(i, w_{\mathrm{p}}, k))) \end{aligned} \tag{26}$$

where, $C_{\mathrm{p}}(i, w_{\mathrm{p}}, k)$ is the hourly sequence number of the $k$-*th* hour contained in the $w_{\mathrm{p}}$-*th* time segment of the $i$-*th* day during SMC simulation. Time segments in a day is graphically shown in Fig. 3. According to (24)-(26), $f_{\mathrm{p}}^*(p)$ will be estimated by SMC simulation. With the decision of $f_{\mathrm{p}}^*(p)$, we can further work out the optimal values of $C_{\mathrm{PV}}^{(\mathrm{r})}$ and $C_{\mathrm{PV}}^{(\mathrm{s})}$ accordingly.

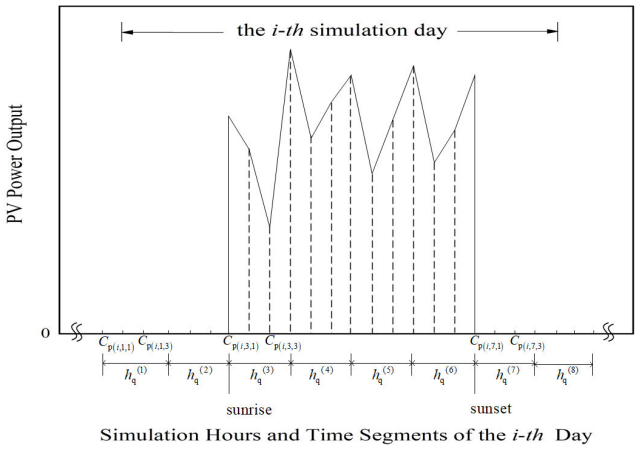


**FIGURE 3.** Intermittent performance of PV. Hours contained by the different time segments are determined and changed when necessary by PDF of *p*.

### E. PROCEDURES OF NSSA

In order to deal with the polymorphic uncertainties of MGs, a NSSA for reliability assessment has been developed to improve the computational efficiency of reliability assessment. As shown in Fig. 4, a preliminary SMC simulation (PSMCS) is assigned to estimate the optimal PDFs of random variables, followed by efficient SMC simulation (ESMCS) to evaluate reliability indices with an accelerated convergence.

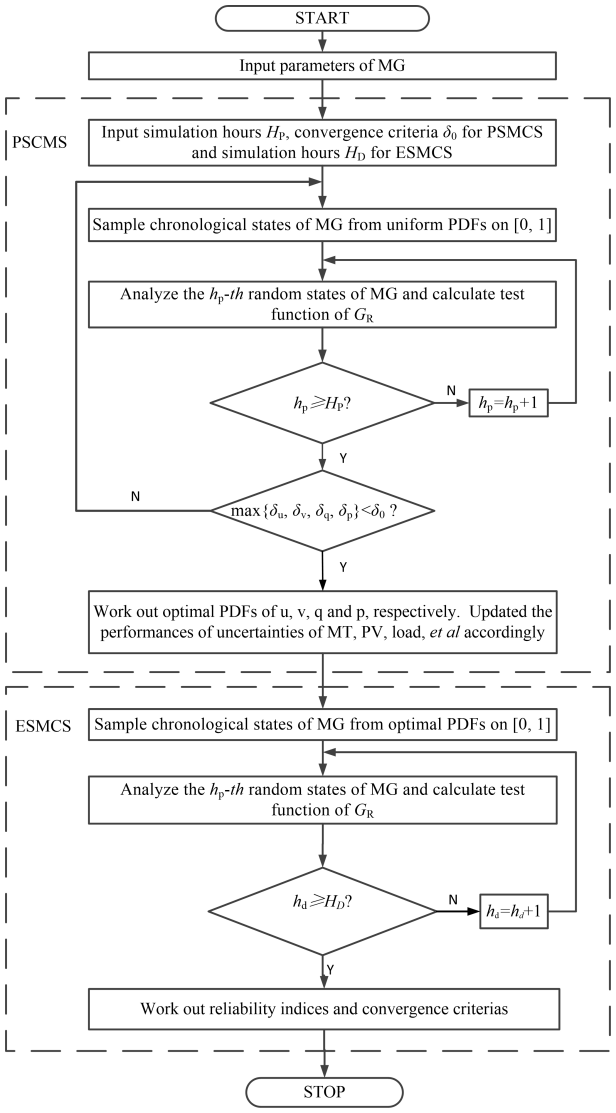


**FIGURE 4.** Flowchart of NSSA for reliability assessment of MG. Optimal PDFs are worked out in PSCMS, then the reliability assessment is implemented with an improved computational efficiency in ESMCS.

It should be noted that, iterative computations are conducted to estimate the optimal PDFs In PSMCS. Iterative errors of PDFs are denoted as $\delta_{\mathrm{u}}$, $\delta_{\mathrm{v}}$, $\delta_{\mathrm{q}}$, and $\delta_{\mathrm{p}}$, and are defined in similar ways. Value of $\delta_{\mathrm{u}}$, for example, can be calculated as follows:

$$\begin{cases} \delta_{\mathrm{u}} = \max\left\{\delta_{\mathrm{u}}^{(1)}, \delta_{\mathrm{u}}^{(2)}, \ldots, \delta_{\mathrm{u}}^{(W_{\mathrm{u}})}\right\} \\ \delta_{\mathrm{u}}^{(w_{\mathrm{u}})} = \dfrac{\tilde{f}_{\mathrm{u}}^*\left(u^{(w_{\mathrm{u}})}\right)^{(\mathrm{n}+1)} - \tilde{f}_{\mathrm{u}}^*\left(u^{(w_{\mathrm{u}})}\right)^{(\mathrm{n})}}{\tilde{f}_{\mathrm{u}}^*\left(u^{(w_{\mathrm{u}})}\right)^{(\mathrm{n})}} \\ (w_{\mathrm{u}} = 1,\ 2,\ \ldots,\ W_{\mathrm{u}}) \end{cases} \tag{27}$$

When $\delta_{\mathrm{u}}$, $\delta_{\mathrm{v}}$, $\delta_{\mathrm{q}}$, and $\delta_{\mathrm{p}}$ get lower than a predetermined convergence criteria $\delta_0$, it is assumed that the optimal PDFs have been worked out.

A NSSA-based reliability assessment program has been coded on the platform of MATLAB. By employing this

program, a test system specified in Section IV is studied, and the convergence performances of traditional SMC and NSSA are thereafter investigated and compared.

## IV. CASE STUDIES

### A. INFORMATION OF TEST SYSTEM

A standalone MG in [7] has been employed as a test system in this work. As shown in Fig. 5, the test system is composed of MT, PV, ESS and 5 load points (LPs), denoted as LP_A, LP_B, LP_C, LP_D and LP_E. It can be seen from Fig. 5 that the polymorphic uncertainties of MG mentioned above have been included. Then a series of case studies based on the test system has been conducted thereby.

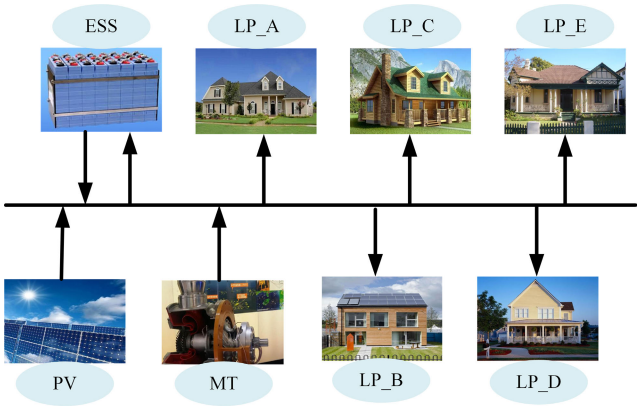


**FIGURE 5.** A schematic diagram of the PV-ESS based standalone MG for case studies. In this test system, polymorphic uncertainties are included.

The following data and assumptions are applied in the case studies.

(1) Annual peak loads of LP_A, LP_B, LP_C, LP_D and LP_E are all equal to 0.3 MW. The percentages of quarterly load in terms of the annual peak load, i.e., $P_{cq}^{(1)}$, $P_{cq}^{(2)}$, $P_{cq}^{(3)}$ and $P_{cq}^{(4)}$ are set to 0.5989, 0.1343, 0.9422 and 0.8081, respectively.

(2) Capacities of MT and PV are set to 1.8 MW and 0.6 MW, respectively. The failure rate, repair rate and repair duration of MT are assumed as 0.25 occurrences per year, 0.125 occurrences per hour and 8 hours respectively. Failure rates of PV are assumed as zero in the following case studies, since intermittency of PV contribute much more to the computational burden than its failure rates.

(3) ESS sizes, i.e., power capacity and energy capacity are set to 0.15 MW and 1 MWh, respectively.

### B. IMPROVEMENT OF COMPUTATIONAL EFFICIENCY

#### 1) CASE 1

In this subsection, the accuracy and convergence performances of NSSA are studied. Take reliability index of LOLP for example. First, a reference value of LOLP has been worked out by conducting a 500-year SMC simulation. Then, the reliability assessments based on traditional SMC simulation and NSSA are implemented, respectively. Computational

**TABLE 1.** Results of LOLP from different simulation years and sampling techniques.

| Simulation years | Results of SMC | Results of NSSA | Errors of SMC (in percent) | Errors of NSSA (in percent) |
|---|---|---|---|---|
| 50 | 0.002538 | 0.002456 | 1.6154 | 1.6694 |
| 60 | 0.002531 | 0.002439 | 1.3433 | 2.3780 |
| 70 | 0.002374 | 0.002520 | 5.1811 | 0.9127 |
| 80 | 0.002406 | 0.002467 | 3.7822 | 1.2161 |
| 90 | 0.002298 | 0.002484 | 8.6597 | 0.5233 |
| 100 | 0.002283 | 0.002497 | 9.3736 | 0.0800 |

results derived from different simulation years are depicted in Fig. 6. The reference value of LOLP which is equal to 0.002497 and denoted by a grey dash line in Fig. 6 provides a benchmark against which the computational accuracy can be measured.

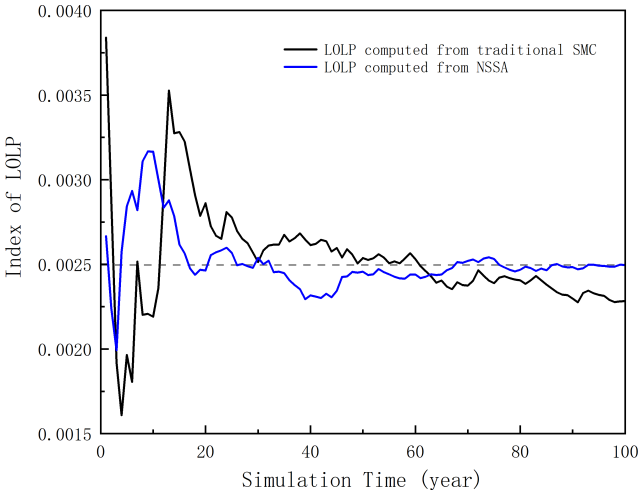


**FIGURE 6.** Curves of LOLP obtained from traditional SMC and NSSA both present convergence along with the increase of simulation years. Compared with traditional SMC, NSSA provides an steadily improved accuracy and depressed oscillation of computational results.

It can be seen from Fig. 6 that computational results of NSSA present depressed oscillation, and thereafter an improved convergence performance is provided. Moreover, the results of LOLP resulted from different simulation years and sampling techniques are listed in Tab. 1.

When the simulation years are small, 50 and 60 for example, computational errors of NSSA are slightly larger than those of SMC, but the differences are marginal. On the other hand, the accuracy of NSSA will get higher steadily than that of SMC as long as the increasement of simulation years. It should be also noted that the computational results of SMC present evident oscillation, which can be depressed to a large extent by NSSA. It is then concluded that compared with traditional SMC simulation, NSSA provides an unbiased estimate of LOLP with an accelerated convergence.

In order to further investigate quantitatively the computational efficiencies, variance and CV of LOLP are worked out and depicted in Fig. 7. It is observed that NSSA can reduce the variance evidently without additional simulation time. Take, for example, simulations of 1, 20 and 100 years. NSSA reduces the variances by 89.7 percent, 87.2 percent and 83.8 percent, respectively on the basis of those resulted from SMC simulation. Due to the reduction of variance, NSSA shows an attractive computational efficiency. For example, CV produced by a 100-year SMC simulation is 0.02221. When NSSA is adopted, only a 12-year simulation is needed to obtain an approximate or even smaller CV (0.02214). Consequently, the computational cost is significantly decreased by NSSA.

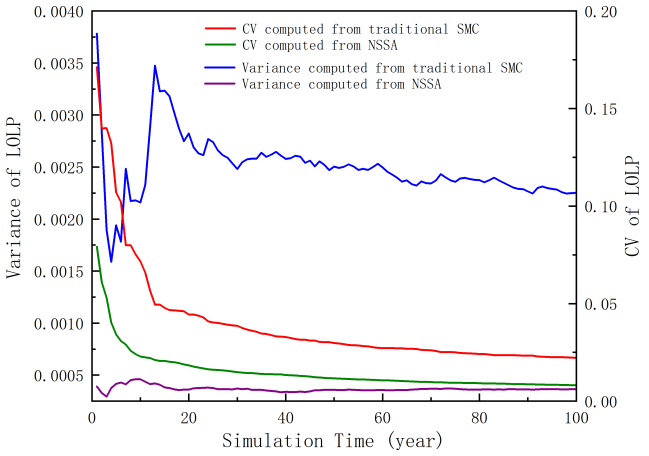


**FIGURE 7.** Variance and CV of LOLP computed by traditional SMC simulation and NSSA. Due to the reduction of CV and variance, NSSA shows attractive computational efficiency.

Furthermore, PDFs of $u$, $v$, $q$ and $p$ are shown in Fig. 8 to explain the reduction of CVs. The uniform PDFs and optimized PDFs are used by traditional SMC simulation and NSSA, respectively. It should be noted in Fig. 8 (a) that, NSSA amplifies PDF of $u$ on the fifth subinterval of [0, 1], then more samples of $TTF(u_i)$ with smaller values will be generated. Meanwhile, NSSA also amplifies PDF of $v$ on the first two subintervals of [0, 1], then more samples of $TTR(v_i)$ with greater values will be generated. As a result, more load deficiency states are prompted and the CVs are then reduced. However, Fig. 8 (b) and (c) also show that PDFs of $q$ and $p$ have not been significantly changed by NSSA, for the variance and CV of LOLP are not dominated by load and PV under the aforementioned system condition. As illustrated in the following subsection, the decisive random variables which dominate variance and CV will be different when system condition changes. Then the adaptability of NSSA will also be validated correspondingly.

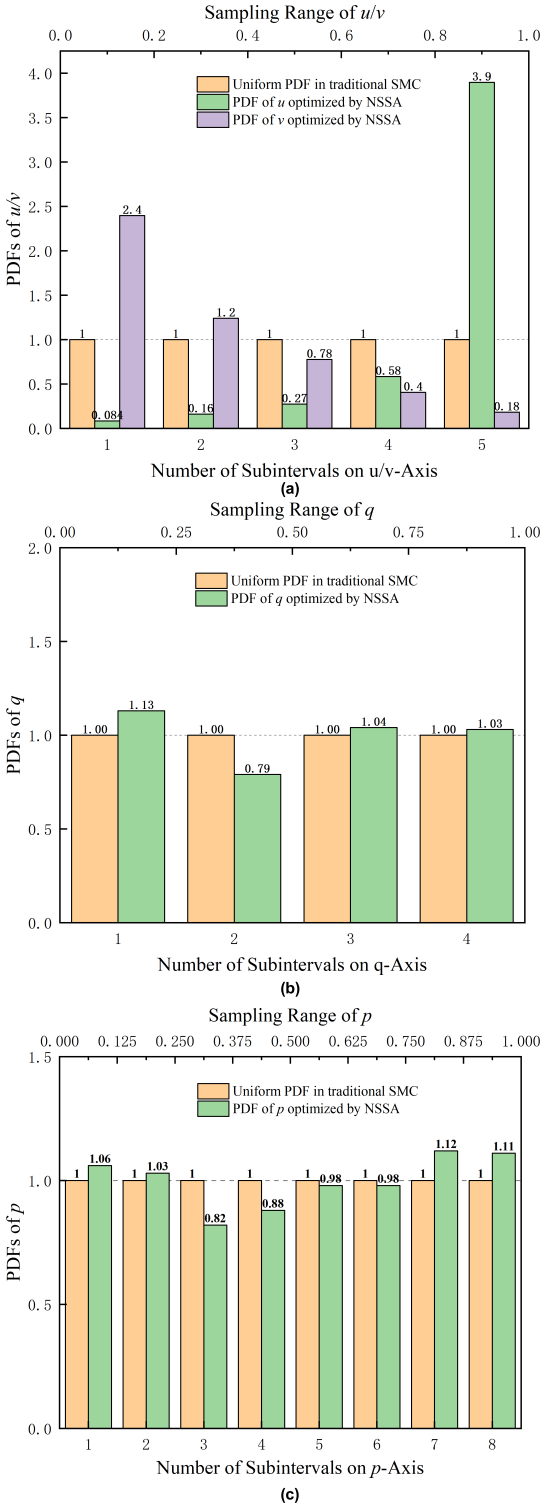


**FIGURE 8.** PDFs of $u$, $v$, $q$ and $p$ on interval [0, 1] used by traditional SMC and NSSA. (a) By concentrating on the fifth subinterval of u-axis, and the first two subintervals of $v$-axis, NSSA provides an improved computational efficiency. PDFs of $q$ shown in (b) and PDFs of $p$ shown in (c) have not been significantly changed, since $q$ and $p$ are not decisive variables under the aforementioned system condition.

### 2) CASE 2

In Case 1, the computational efficiency essentially produced by $f_u^*(u)$ and $f_v^*(v)$ has been confirmed. In this case, loads and capacities of MT and PV are changed for further investigations. Firstly, annual peak loads of LP_A, LP_B, LP_C, LP_D and LP_E grow from 0.3 MW to 0.5 MW. Secondly, penetration level of PV is increased by setting the

**TABLE 2. Computational results of traditional SMC simulation and NSSA.**

| Items | SMC | NSSA | Difference (in percent) |
|---|---|---|---|
| LOLP | 0.280 | 0.284 | 1.43 |
| Variance of LOLP | 0.201 | 0.085 | -57.71 |
| CV of LOLP | 0.0038 | 0.0024 | -36.84 |

capacity of MT to 1.2 MW instead of 1.8 MW, and setting the capacity of PV to 1.2 MW instead of 0.6 MW. We conduct reliability studies on the test system based on traditional SMC simulation and NSSA, respectively. Computational results of LOLP, variance and CV are listed in Tab. 2.

The results in Tab. 2 show that an unbiased LOLP and significant improvement in computational efficiency are provided by NSSA under a system condition different from that in Case 1. Optimal PDFs of $u$, $v$, $q$ and $p$ produced by NSSA are graphically shown in Fig. 9.

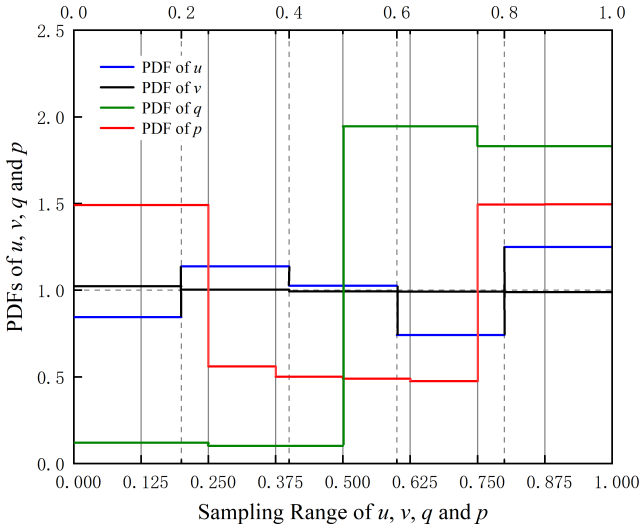


**FIGURE 9. PDFs of *u*, *v*, *q* and *p* used by NSSA. PDFs of *u* and *v* slightly deviate from 1 on the interval of [0, 1], however, PDFs of *q* and *p* show significant deviation from 1.**

It can be seen from Fig. 9 that optimal PDFs of $q$ and $p$ deviate much farther from 1 than those of $u$ and $v$. In other words, load and PV dominate the variance and CV of LOLP, and therefore $f_q^*(q)$ and $f_p^*(p)$ mainly account for the improvement of computational efficiency. Please note that, optimization of PDFs of $q$ and $p$ results in modified load profile, and changed sunrise and sunset time, respectively. $h_q^{(1)}$, $h_q^{(2)}$, $h_q^{(3)}$ and $h_q^{(4)}$ are set to 263 hours, 225 hours, 4261 hours and 4011 hours instead of 2190 hours according to $f_q^*(q)$. Meanwhile, $C_{PV}^{(r)}$ and $C_{PV}^{(s)}$ are set to 8:00 and 14:00 instead of 6:00 and 18:00 according to $f_p^*(p)$. Consequently, more random states of MG with heavy load and little PV power are then produced. In other words, the computational efficiency is thereby improved due to the reduction of ineffective samples of random states.

### C. SCENARIO-BASED RELIABILITY ANALYSIS

In this work, NSSA is developed not only to improve the computational efficiency, but also to conduct the scenario-based reliability analysis. It can be seen from (17), (21) and (24) that the optimal PDFs produced by NSSA are positively relevant to the test functions of reliability indices. Moreover, the case studies mentioned above show that optimal PDFs of dominant random variables will deviate from 1 much farther than other random variables. Then, a novel index, i.e., DJ-PDF is defined as the product of optimal PDFs of dominant random variables to quantitatively measure the contribution of different scenarios to the reliability indices. Take for example, Case 2 in Subsection B. The dominant random variables are $q$ and $p$, and DJ-PDF are worked out as follows.

$$D_{JPDF}(w_q, w_p) = \tilde{f}_q^*(q^{(w_q)}) \times \tilde{f}_p^*(p^{(w_p)}) \tag{28}$$

where, $D_{JPDE}(w_q, w_p)$ is the DJ-PDF value of point $(w_q, w_p)$. Here, $w_q$ denotes the $w_q$-th subinterval of [0, 1] on $q$-axis and also corresponds to quarter-$w_q$. Similarly, $w_p$ denotes the $w_p$-th subinterval of [0, 1] on $p$-axis and also corresponds to the $w_p$-th time segment. Note that every time segment includes 3 hours since one day is divided into 8 time segments. As an example, $D_{JPDE}(1, 2)$ denotes the DJ-PDF over time segment from 3:00 to 6:00, in quarter-1. DJ-PDF of Case 2 in Subsection B is worked out and shown in Fig. 10.

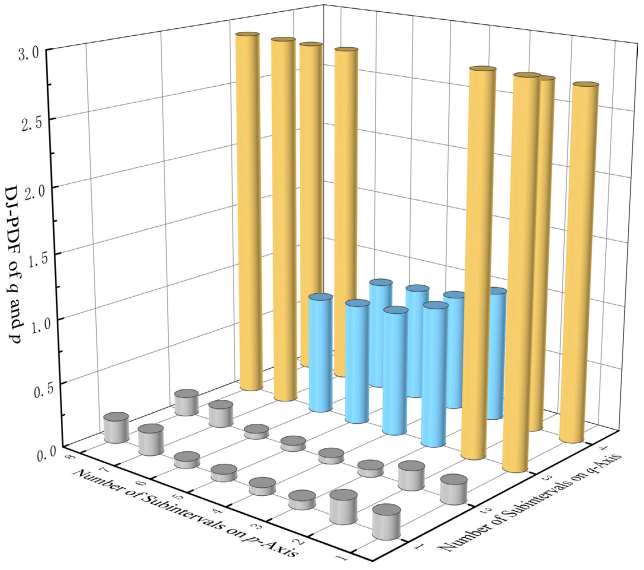


**FIGURE 10. DJ-PDF of *q* and *p* produced by NSSA. Values of DJ-PDF in quarter-3 and quarter-4 are larger than those in quarter-1 and quarter-2, and Values of DJ-PDF in the 3*rd*, 4*th*, 5*th* and 6*th* time segments are smaller than those in other time segments.**

As presented in Fig. 10, DJ-PDF varies according to quarters and time segments. In quarter-1 and quarter-2, DJ-PDF is small due to that the load is light. However, in quarter-3 and quarter-4, DJ-PDF is evidently increased, since the load is heavy. In addition, values of DJ-PDF of the 3*rd*, 4*th*, 5*th* and 6*th* time segments which correspond to sunshine time are smaller than those of other time segments due to the

**TABLE 3.** DJ-PDFs and corresponding load interruption percentages.

| Quarters | Time segments | DJ-PDFs | Load Interruptions (in percent) |
|---|---|---|---|
| 1 | 1 | 0.1794 | 0.0532 |
| 1 | 3 | 0.0674 | 0.0470 |
| 1 | 7 | 0.1798 | 0.0490 |
| 3 | 1 | 2.9019 | 11.1456 |
| 3 | 3 | 1.0900 | 2.5169 |
| 3 | 7 | 2.9085 | 11.1456 |

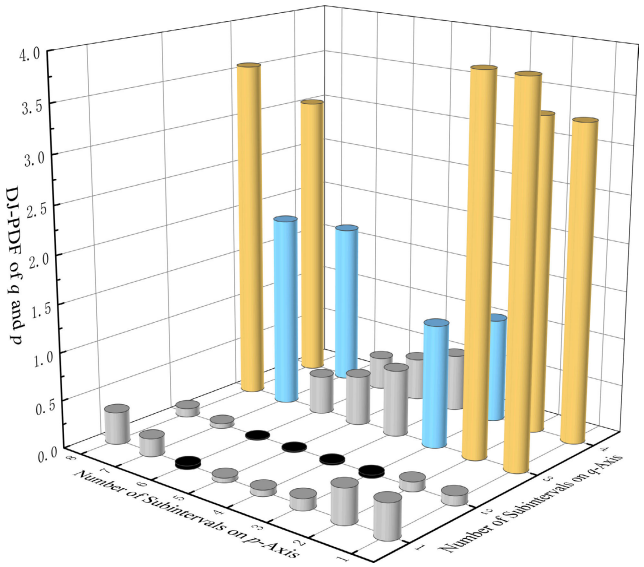


**FIGURE 11.** DJ-PDF of $q$ and $p$ when ESS capacities are increased. Due to the contribution of ESS, DJ-PDF moves downwards constantly during sunshine time, and moves upwards after sunset.

contribution of PV power. The validity of DJ-PDF can be confirmed by Tab. 3, in which the DJ-PDF and percentages of load interruptions in several scenarios are listed.

Tab. 3 has well illustrated that DJ-PDF can be employed to quantitatively measures the risk of load interruption in different scenarios. For example, time segments 1 and 7 of quarter-3 both account for two largest percentages, i.e., 11.1456% of all the load interruptions during the simulation years. Meanwhile, the corresponding DJ-PDFs in the same scenarios are 2.9019 and 2.9085, which are also the first two largest values of DJ-PDFs. Consequently, the scenarios with low or high risk of load interruption can be identified by DJ-PDF. Adaptability of DJ-PDF is further investigated by increasing ESS capacities. Assume that power capacity and energy capacity of ESS are increased to 1.5 MW and 3 MWh, respectively. DJ-PDF is then worked out and depicted as follows.

The similarities between Fig. 10 and Fig. 11 can be found. First, DJ-PDFs of quarter-3 and quarter-4 are greater than those of quarter-1 and quarter-2. Second, DJ-PDFs of the time segments with sunshine is smaller than those of other time segments. However, it is also worth mentioning the differences between Fig. 10 and Fig. 11. Take DJ-PDFs in quarter-3 for example. During sunshine time, DJ-PDFs in Fig. 10 are 1.09, 0.98, 0.95 and 0.93, which show marginal differences. On the contrary, DJ-PDFs in Fig. 11 are 1.28, 0.70, 0.52 and 0.40, and move downwards constantly. The downward trend of DJ-PDFs during the sunshine time in Fig. 11 can be explained when ESS is considered. The contribution of ESS to consistent power supply is increased continuously during sunshine time, since more redundant PV energy will be absorbed by ESS before sunset. As a result, the minimum value of DJ-PDF is obtained in the 6*th* time segment. Finally, it should also be noted in Fig. 11 that DJ-PDF in the 7*th* time segment is smaller than that in the 8*th* time segment, due to that residual energy of ESS reduces the probability of load shedding in the 7*th* time segment.

## V. CONCLUSION

The polymorphic uncertainties in MGs, such as stochastic and chronological operation cycles of MT, intermittency of PV and varying profile of load, etc. produce prohibitive computational cost for reliability assessment. In this work, a novel sampling technique with high efficiency, i.e., NSSA is developed to reduce the computational cost. A series of case studies have been conducted, and not only the capability of NSSA to improve the computational efficiency but also its adaptability to system conditions are then confirmed. Moreover, DJ-PDF is defined as the product of optimal PDFs and employed to quantify the contributions of different scenarios to the reliability indices. Therefore, DJ-PDF can be produced by NSSA and further applied for scenario-based reliability analysis, which will provide detailed reliability information complementary to the conventional reliability indices.

## REFERENCES

[1] W. Zhong, L. Wang, Z. Liu, and S. Hou, "Reliability evaluation and improvement of islanded microgrid considering operation failures of power electronic equipment," *J. Modern Power Syst. Clean Energy*, vol. 8, no. 1, pp. 111–123, 2020, doi: 10.35833/MPCE.2018.000666.

[2] A. Hirsch, Y. Parag, and J. Guerrero, "Microgrids: A review of technologies, key drivers, and outstanding issues," *Renew. Sustain. Energy Rev.*, vol. 90, pp. 402–411, Jul. 2018.

[3] P. Wei and W. Chen, "Microgrid in China: A review in the perspective of application," *Energy Procedia*, vol. 158, pp. 6601–6606, Feb. 2019.

[4] X. Xu, J. Mitra, T. Wang, and L. Mu, "Evaluation of operational reliability of a microgrid using a short-term outage model," *IEEE Trans. Power Syst.*, vol. 29, no. 5, pp. 2238–2247, Sep. 2014.

[5] A. M. LeitedaSilva, W. F. Schmitt, A. M. Cassula, and C. E. Sacramento, "Analytical and Monte Carlo approaches to evaluate probability distributions of interruption duration," *IEEE Trans. Power Syst.*, vol. 20, no. 3, pp. 1341–1348, Aug. 2005.

[6] K. Hou, H. Jia, X. Xu, Z. Liu, and Y. Jiang, "A continuous time Markov chain based sequential analytical approach for composite power system reliability assessment," *IEEE Trans. Power Syst.*, vol. 31, no. 1, pp. 738–748, Jan. 2016.

[7] X. Song, Y. Zhao, J. Zhou, and Z. Weng, "Reliability varying characteristics of PV-ESS-Based standalone microgrid," *IEEE Access*, vol. 7, pp. 120872–120883, 2019.

[8] P. M. de Quevedo, J. Contreras, A. Mazza, G. Chicco, and R. Porumb, "Reliability assessment of microgrids with local and mobile generation, time-dependent profiles, and intraday reconfiguration," *IEEE Trans. Ind. Appl.*, vol. 54, no. 1, pp. 61–72, Jan. 2018.

[9] S. Wang, X. Zhang, and L. Liu, "Multiple stochastic correlations modeling for microgrid reliability and economic evaluation using pair-copula function," *Int. J. Electr. Power Energy Syst.*, vol. 76, pp. 44–52, Mar. 2016.
[10] Z. Liu, W.-L. Liu, G.-C. Su, H. Yang, and G. Hu, "Wind-solar micro grid reliability evaluation based on sequential Monte Carlo," in *Proc. Int. Conf. Probabilistic Methods Appl. Power Syst. (PMAPS)*, Beijing, China, Oct. 2016, pp. 1–6.
[11] R. R. Micky, R. Lakshmi, R. Sunitha, and S. Ashok, "Generation adequacy assessment for microgrid with ESS," in *Proc. IEEE 7th Power India Int. Conf. (PIICON)*, Bikaner, India, Nov. 2016, pp. 1–6.
[12] P. Gautam, R. Karki, and P. Piya, "Probabilistic modeling of energy storage to quantify market constrained reliability value to active distribution systems," *IEEE Trans. Sustain. Energy*, vol. 11, no. 2, pp. 1043–1053, Apr. 2020, doi: 10.1109/TSTE.2019.2917374.
[13] A. M. Leite da Silva, L. C. Nascimento, A. C. R. Guimaráes, and J. C. O. Mello, "Reliability indices applied to performance-based mechanisms in electric power distribution systems," *Int. J. Syst. Assurance Eng. Manage.*, vol. 1, no. 2, pp. 105–112, Jun. 2010.
[14] P. Wang and R. Billinton, "Time sequential distribution system reliability worth analysis considering time varying load and cost models," *IEEE Trans. Power Del.*, vol. 14, no. 3, pp. 1046–1051, Jul. 1999.
[15] A. Ali Kadhem, N. I. Abdul Wahab, I. Aris, J. Jasni, and A. N. Abdalla, "Computational techniques for assessing the reliability and sustainability of electrical power systems: A review," *Renew. Sustain. Energy Rev.*, vol. 80, pp. 1175–1186, Dec. 2017.
[16] N. Li, X. Wang, Z. Zhu, and C. Gu, "Reliability evaluation of power system based on isodisperse important sampling method and dynamic parallel calculation," *Energy Procedia*, vol. 156, pp. 343–348, Jan. 2019.
[17] J. Cai, Q. Xu, M. Cao, and B. Yang, "A novel importance sampling method of power system reliability assessment considering multi-state units and correlation between wind speed and load," *Int. J. Electr. Power Energy Syst.*, vol. 109, pp. 217–226, Jul. 2019.
[18] S. Zhong, T. Yang, Y. Wu, S. Lou, and T. Li, "The reliability evaluation method of generation system based on the importance sampling method and states clustering," *Energy Procedia*, vol. 118, pp. 128–135, Aug. 2017.
[19] D. Li, L. Dong, H. Shen, B. Li, and Y. Liao, "Reliability evaluation of composite generation and transmission systems based on stratified and gradual importance sampling algorithm," in *Proc. APAP*, Beijing, China, Oct. 2011, pp. 2082–2087.
[20] X. Song and Z. Tan, "Power system reliability evaluation based on optimal sampling and selective analysis algorithm," *Autom. Electr. Power Syst.*, vol. 33, no. 5, pp. 29–33, Mar. 2009.
[21] R. Billinton and W. Wangdee, "Impact of utilising sequential and non-sequential simulation techniques in bulk-electric-system reliability assessment," *Gener., Transmiss. Distrib.*, vol. 152, no. 5, pp. 623–628, Sep. 2005.
[22] W. Wangdee and R. Billinton, "Reliability-performance-index probability distribution analysis of bulk electricity systems," *Can. J. Electr. Comput. Eng.*, vol. 30, no. 4, pp. 189–193, 2005.
[23] R. Billinton, S. Kumar, N. Chowdhury, K. Chu, K. Debnath, L. Goel, E. Khan, P. Kos, G. Nourbakhsh, and J. Oteng-Adjei, "A reliability test system for educational purposes-basic data," *IEEE Trans. Power Syst.*, vol. 4, no. 3, pp. 1238–1244, Aug. 1989.
[24] X. Song, W. Xu, J. Zhou, Y. Sun, and W. Zheng, "Selective data-driven algorithm proposed for reliability evaluation of microgrid with sequential multi-state uncertainties," *High Voltage Eng.*, vol. 46, no. 7, pp. 2370–2379, Jul. 2020.
[25] H. Moradi, M. Esfahanian, A. Abtahi, and A. Zilouchian, "Modeling a hybrid microgrid using probabilistic reconfiguration under system uncertainties," *Energies*, vol. 10, no. 9, p. 1430, Sep. 2017.
[26] R. Billinton and R. Allan, *Reliability Evaluation of Power Systems*. New York, NY, USA: Plenum, 1996.
[27] J. P. Hop and H. K. Dijk, "SISAM and MIXIN: Two algorithms for the computation of posterior moments and densities using Monte Carlo integration," *Comput. Sci. Econ. Manage.*, vol. 5, no. 3, pp. 183–220, Aug. 1992.
[28] R. A. Gonzalez-Fernandez, R. E. Oviedo-Sanabria, and A. M. L. da Silva, "Generating capacity reliability assessment of the itaipu hydroelectric plant via sequential Monte Carlo simulation," in *Proc. Power Syst. Comput. Conf.*, Aug. 2014, pp. 1–7.

**XIAOTONG SONG** received the B.Eng. and Ph.D. degrees in electrical engineering from Shandong University, Jinan, China, in 2003 and 2008, respectively.

He was a Senior Engineer with the China Electric Power Research Institute (CEPRI). He is currently an Associate Professor with the School of Electrical and Control Engineering, North China University of Technology (NCUT), Beijing, China. His research interests include power system reliability assessment, microgrid, and energy storage systems.

Dr. Song was a recipient of the Grand Prize of State Grid Awards for Science and Technology Progress, in 2013.

**YI SUN** was born in Beijing, China, in 1997. He received the B.Eng. degree in electrical engineering and automation from the North China University of Technology (NCUT), in 2019, where he is currently pursuing the M.S. degree in electrical engineering. His research interests include optimized scheduling of microgrid and distributed generation.

**FEI WANG** received the B.Eng. and M.S. degrees in electrical engineering from Shandong University, China, in 2003 and 2007, respectively. He is currently a Senior Engineer with State Grid Shandong Electric Power Company. His research interests include power system reliability analysis and power grid planning.

**WENYUE XU** was born in Beijing, China, in 1995. She received the B.Eng. degree in electrical engineering and its automation from the Beijing Institute of Petrochemical Technology, in 2018. She is currently pursuing the M.S. degree in electrical engineering with the North China University of Technology (NCUT). Her research interest includes reliability assessment of microgrid.